

Mixed-isotope Bose-Einstein condensates in Rubidium

Valery S. Shchesnovich^{1,*} Anatoly M. Kamchatnov^{1,2,†} and Roberto A. Kraenkel^{1‡}

¹*Instituto de Física Teórica, Universidade Estadual Paulista-UNESP,*

Rua Pamplona 145, 01405-900 São Paulo, Brazil

²*Institute of Spectroscopy, Russian Academy of Sciences,*

Troitsk 142190, Moscow Region, Russia

(Dated: December 19, 2019)

Abstract

We consider the ground state properties of mixed Bose-Einstein condensates of ^{87}Rb and ^{85}Rb atoms in the isotropic pancake trap, for both signs of the interspecies scattering length. In the case of repulsive interspecies interaction, there are symmetry preserving and symmetry breaking ground states. The threshold for the symmetry breaking transition, which is related to appearance of a zero dipole-mode, is found numerically. For attractive interspecies interactions, the two condensates assume symmetric ground states for the numbers of atoms up to the collapse instability of the mixture.

PACS numbers: PACS: 03.75.Mn, 03.75.Hh

Keywords: Bose-Einstein condensates, mixtures of quantum gases, symmetry breaking

*Electronic address: valery@ift.unesp.br

†Electronic address: kamch@isan.troitsk.ru

‡Electronic address: kraenkel@ift.unesp.br

I. INTRODUCTION

Bose-Einstein condensation (BEC) in mixtures of trapped quantum gases has become an exciting field of study. First experimental observation of the two-species BEC was realized for two different spin states of ^{87}Rb [1]. The overlapping condensates of ^{87}Rb in the spin states $|F = 1, m = -1\rangle$ and $|F = 2, m = 2\rangle$ were created via nearly lossless sympathetic cooling of the atoms in the state $|2, 2\rangle$ by thermal contact with the atoms in the $|1, -1\rangle$ -state. Also, the double-condensate system of ^{87}Rb in the spin states $|1, -1\rangle$ and $|2, 1\rangle$ was created from the condensate in the $|1, -1\rangle$ -state by driving a two-photon transition [2]. In the subsequent evolution after creation, the condensates underwent complex relative motions preserving the total density profile. The motions quickly damped out and the condensates assumed a steady state with a non-negligible (and adjustable) overlap region. These experiments started a series of works devoted to experimental and theoretical study of BEC in mixtures. For instance, superposition of the spinor condensates of ^{23}Na led to observation of weakly miscible and immiscible superfluids [3] and occurrence of the metastable states [4]. Interaction between two condensates of different spin states of ^{87}Rb in the displaced traps was observed in the center-of-mass oscillations [5]. Finally, the mixed BEC of two different atom species, ^{41}K and ^{87}Rb , [6] and the Fermi sea of ^6Li coexisting with a large ^{23}Na condensate [7] were experimentally produced.

A promising combination for obtaining the two-species BEC potentially rich in new phenomena is the mixture of two isotopes of Rubidium: ^{85}Rb and ^{87}Rb . There is a long standing interest in obtaining this BEC mixture, which goes back to Ref. [8], where the feasibility of achieving such two-species BEC was established. It was suggested that condensation of the two isotopes of Rubidium can be achieved via the sympathetic cooling of certain hyperfine states which exhibit low inelastic collision rates. Moreover, the possibility of employing the Feshbach resonance for control over the scattering length was stressed. The optimal combination was found to be the mixture of the spin states $|2, -2\rangle_{85}$ and $|1, -1\rangle_{87}$, because the scattering length *between* the isotopes can be controlled. The sympathetic cooling of the ^{85}Rb condensate by thermal contact with the ^{87}Rb condensate was subsequently experimentally demonstrated [9]. Up to 10^6 atoms of the ^{85}Rb isotope were cooled via elastic collisions with a large reservoir (10^9 atoms) of ^{87}Rb . The stable condensate of the ^{85}Rb isotope was also created by using the Feshbach resonance to reverse the sign of the scattering length

from negative to positive [10]. In this way, the long-living condensates with up to 10^4 atoms of ^{85}Rb in the spin state $|2, -2\rangle$ were produced.

One of the principal advantages of using the Rubidium isotopes is that their interspecies and intraspecies scattering lengths are known with a good precision [8], thus theoretical predictions can be compared with the experiment. In particular, the scattering lengths of the ^{87}Rb isotope and between the two isotopes are positive, while the scattering length of the ^{85}Rb isotope is negative.

It is worth noting that in all the previous experiments on the BEC mixtures the interspecies as well as intraspecies interactions were repulsive. With few exceptions (discussed below), only the mixtures of condensates with repulsive interactions in each of the species were considered from the theoretical point of view. The following criterion for the spatial separation of a mixture of two repulsive condensates was derived for BEC in a box [11]: if the mutual repulsion is large enough, i.e., $G_{12} > \sqrt{G_{11}G_{22}}$ (where G_{ij} is the interaction coefficient), the condensates separate to lower the energy. The symmetry breaking point of view on the ground state in the mixture of condensates was developed in Refs. [12, 13, 14, 15, 16]. For instance, by taking equal number of atoms in the two species, the symmetry-preserving vs. symmetry-breaking phase diagram was obtained in Ref. [14]. Existence of the metastable states in the BEC mixtures was argued also on the basis of the Bogoliubov excitation spectrum in Ref. [17], where both signs of the interspecies scattering length were considered (for repulsive intraspecies interactions). In Ref. [18] the two-component condensates with coinciding positive or negative interspecies scattering lengths and equal numbers of atoms were considered within a variational approach. However, the results of the latter work do not apply to the BEC mixture of two isotopes of Rubidium, where, first of all, the interspecies scattering lengths have different signs. Finally, the multi-component collapse in a spherically symmetric trap was studied numerically in Ref. [20], with application to the two-species and hybrid atomic-molecular BEC of ^7Li , where the all possible combinations the signs of atomic interactions for the two species were considered. It was found that either one or both components of the multi-component BEC may experience collapse depending on the interaction coefficients.

In the present paper we study two-species BEC in a pancake trap, for the numbers of atoms below the collapse instability. Our main goal is to understand the ground state of the two-species BEC mixture comprised of the ^{85}Rb and ^{87}Rb isotopes, with the atoms

being in the optimal spin states, $|2, -2\rangle_{85}$ and $|1, -1\rangle_{87}$. We consider both the attractive and the repulsive interspecies interactions for fixed (default) intraspecies interactions with the scattering lengths: -412.5 a.u. (-21.8 nm) for $|2, -2\rangle_{85}$ and 107.5 a.u. (5.7 nm) for $|1, -1\rangle_{87}$ —the averages of those given in Ref. [8]. In section II we introduce the two-dimensional model describing the two-species BEC mixture in a pancake trap and discuss the domain of its applicability. Then, we present the numerically found ground states in the BEC mixture of the two isotopes of Rubidium for the repulsive as well as attractive interspecies interactions, sections III A and III B, respectively. The concluding section IV contains brief summary of the results. Detailed derivation of the two-dimensional model is placed in appendix A, while details of the stability analysis of the axially symmetric ground states are given in appendix B.

II. TWO-DIMENSIONAL MODEL FOR THE PANCAKE TRAP

We consider two-species BEC mixture in the isotropic pancake trap for arbitrary intraspecies and interspecies scattering lengths. The Gross-Pitaevskii equations for the two-species BEC have the following form:

$$i\hbar\partial_t\Psi_1 = -\frac{\hbar^2}{2m_1}\nabla^2\Psi_1 + V_1(\mathbf{r})\Psi_1 + (G_{11}|\Psi_1|^2 + G_{12}|\Psi_2|^2)\Psi_1, \quad (1a)$$

$$i\hbar\partial_t\Psi_2 = -\frac{\hbar^2}{2m_2}\nabla^2\Psi_2 + V_2(\mathbf{r})\Psi_2 + (G_{22}|\Psi_2|^2 + G_{12}|\Psi_1|^2)\Psi_2, \quad (1b)$$

where $\Psi_1(\mathbf{r}, t)$ and $\Psi_2(\mathbf{r}, t)$ are the order parameters of the two species, while the interaction coefficients are given as $G_{11} = 4\pi\hbar^2 a_1/m_1$, $G_{22} = 4\pi\hbar^2 a_2/m_2$, and $G_{12} = 2\pi\hbar^2 a_{12}/M$, with a_1 , a_2 and a_{12} being the intraspecies and the interspecies scattering lengths, respectively. Here M denotes the reduced mass: $M = m_1 m_2 / (m_1 + m_2)$. In our case, for the two isotopes of Rubidium, we can neglect the mass difference between the isotopes and take $m = m_1 = m_2$. We consider the parabolic pancake trap,

$$V_j = \frac{m\omega_{j,z}^2}{2}z^2 + \frac{m\omega_{j,\perp}^2}{2}r_\perp^2, \quad j = 1, 2, \quad (2)$$

with strong confinement in z -direction: $\gamma \equiv \omega_z/\omega_\perp \gg 1$ (by a simple phase transformation the possible difference of the zero-point energies for the two species in the trap can be scaled away from the system (1)). The difference in the magnetic trap frequencies felt by the two species is caused by the difference of the Lande magnetic factors for the two

isotopes [19]: $g(|2, -2\rangle_{85}) = -1/6$ and $g(|1, -1\rangle_{87}) = -1/4$. The corresponding magnetic moments measured in the Bohr magnetons are given as follows: $\mu_{85} = g(|2, -2\rangle_{85})m_{85} = 1/3$ and $\mu_{87} = g(|1, -1\rangle_{87})m_{87} = 1/4$. Hence, the ratio of the squared trap frequencies is $\omega_{87}^2/\omega_{85}^2 = \mu_{87}/\mu_{85} = 3/4$, where ω_{85} and ω_{87} stand for the frequencies experienced by the respective isotopes. From now on, the indices 1 and 2 will correspond to the isotopes ^{85}Rb and ^{87}Rb , respectively.

For not too large numbers of atoms the three-dimensional system (1) can be reduced to a system of two-dimensional equations in the pancake coordinates $\mathbf{r}_\perp = (x, y)$, while the order parameter in z -direction is fixed and given by the Gaussian. Indeed, the motion in z -direction is quantized under the condition that the energy contribution from the nonlinearity is much less than the difference between the energy levels of the trap in z -direction:

$$\frac{|G_{j1}|N_1}{d_{1,z}d_{1,\perp}^2} \ll \hbar\omega_{1,z}, \quad \frac{|G_{j2}|N_2}{d_{2,z}d_{2,\perp}^2} \ll \hbar\omega_{2,z}, \quad j = 1, 2. \quad (3)$$

Here we have estimated the order parameter as $|\Psi_j|^2 \sim N_j/(d_{j,z}d_{j,\perp}^2)$, $j = 1, 2$, with introduction of the effective sizes of the condensates in the pancake plane ($d_{j,\perp}$) and in z -direction ($d_{j,z}$). Under the condition (3), the z -sizes of the condensates are given by the trap size: $d_{j,z} = a_{j,z}$, with $a_{j,z}$ being the respective oscillator length in z -direction (see formula (4)). Whereas their sizes in the pancake plane must be determined from the solution to the resulting two-dimensional system (system (6) below). We will reformulate the condition (3) in a more convenient form below. More detailed analysis of the two-dimensional approximation is placed in appendix A.

Under the condition (3) the order parameter Ψ_j , $j = 1, 2$, is approximated as a product of the Gaussian wave function in z -direction and a wave function describing the transverse shape:

$$\Psi_j = e^{-i\omega_{j,z}t/2} f_j(z) \Phi_j(\mathbf{r}_\perp, t), \quad f_j \equiv \pi^{-1/4} a_{j,z}^{-1/2} \exp\left(-\frac{z^2}{2a_{j,z}^2}\right), \quad a_{j,z} \equiv \left(\frac{\hbar}{m\omega_{j,z}}\right)^{1/2}. \quad (4)$$

The Gaussian is the ground state wave-function of the linear parts of the r.h.s.'s in equations (1) which correspond to the quantum motion in z -direction: $H_{j,z} \equiv -\hbar^2/(2m)\partial_z^2 + m\omega_{j,z}^2 z^2/2$, with $H_{j,z}f_j(z) = (\hbar\omega_{j,z}/2)f_j(z)$. Substitution of the expression (4) in the system (1), multiplication of the equation for Ψ_j by $f_j(z)$ and integration over z results in the approximate two-dimensional system (see also equations (A3)-(A4) from appendix A). To write it down in a form convenient for numerical calculations, let us introduce the dimensionless variables:

$$\boldsymbol{\rho} = \frac{\mathbf{r}_\perp}{a_\perp}, \quad a_\perp \equiv \left(\frac{\hbar}{m\omega_\perp} \right)^{1/2}, \quad T = \frac{\omega_\perp}{2}t, \quad \psi_j = a_\perp \Phi_j, \quad j = 1, 2. \quad (5)$$

Here we have defined the frequency ω_\perp as $\omega_\perp^2 = (\omega_{1,\perp}^2 + \omega_{2,\perp}^2)/2$, where $\omega_{j,\perp}$, $j = 1, 2$, are the trap frequencies in the pancake plane experienced by the two isotopes. Then the dimensionless approximate 2D system reads:

$$i\partial_T \psi_1 = -\nabla_\perp^2 \psi_1 + \lambda_1^2 \rho^2 \psi_1 + (g_{11}|\psi_1|^2 + g_{12}|\psi_2|^2)\psi_1, \quad (6a)$$

$$i\partial_T \psi_2 = -\nabla_\perp^2 \psi_2 + \lambda_2^2 \rho^2 \psi_2 + (g_{22}|\psi_2|^2 + g_{12}|\psi_1|^2)\psi_2, \quad (6b)$$

where $\rho = |\boldsymbol{\rho}|$,

$$g_{11} = \frac{4\sqrt{2\pi}a_1}{a_{1,z}}, \quad g_{22} = \frac{4\sqrt{2\pi}a_2}{a_{2,z}}, \quad g_{12} = \frac{8\sqrt{\pi}a_{12}}{(a_{1,z}^2 + a_{2,z}^2)^{1/2}}, \quad \lambda_1 = \frac{\omega_{1,\perp}}{\omega_\perp}, \quad \lambda_2 = \frac{\omega_{2,\perp}}{\omega_\perp}. \quad (7)$$

Using the relation $\omega_2^2/\omega_1^2 = 3/4$ for the Rubidium isotopes in the spin states $|2, -2\rangle_{85}$ and $|1, -1\rangle_{87}$, we obtain: $\lambda_1^2 = 8/7$ and $\lambda_2^2 = 6/7$.

The pancake trap sizes in the experiments on BEC have different values. To set a reference for discussion, in the calculations below we assume the z -size of the trap to be $10\mu\text{m}$, i.e., we set $a_{1,z} = 10\mu\text{m}$ ($a_{2,z} = 2.03^{-1/4}a_{1,z} = 0.84a_{1,z}$). This results in the following values for the interaction coefficients in the mixture of the two isotopes of Rubidium: $g_{11} = -0.0219$, $g_{22} = 0.0068$, and $g_{12} = 0.012$. For a different trap size the interaction coefficients will change. However, the quantities $g_{11}N_1$, $g_{22}N_2$, $g_{12}N_2$, and $g_{12}N_1$, computed on a solution to the system (6), will remain invariant under the variation of the trap size. Thus, a different trap size a_z will result in a similar solution but for the appropriately scaled numbers of atoms. We will return to this point below.

Let us now reformulate the conditions (3) in a form more convenient for verification. Scaling the sizes of the condensates in the pancake plane by the respective trap length, $d_{j,\perp} = R_j a_\perp$, we obtain the equivalent conditions in the form of the bounds on the numbers of atoms:

$$N_1 \ll \gamma \frac{R_1^2}{4\pi} \min \left(\frac{a_z}{|a_1|}, \frac{a_z}{|a_{12}|} \right), \quad N_2 \ll \gamma \frac{R_2^2}{4\pi} \min \left(\frac{a_z}{|a_2|}, \frac{a_z}{|a_{12}|} \right), \quad (8)$$

where a_z denotes both $a_{1,z}$ and $a_{2,z}$, since they have close values, and $\gamma \gg 1$ ($\gamma = \omega_z/\omega_\perp = a_\perp^2/a_z^2$). The sizes R_1 and R_2 of the two condensates must be determined from the solution of the system (6). For instance, for the pancake trap with $a_z = 10\mu\text{m}$, using the values of the scattering lengths from section I for the $^{85}\text{Rb} - ^{87}\text{Rb}$ mixture, we obtain the following

bounds: $N_j \ll 10^2 \gamma R_j^2$, $j = 1, 2$. The actual bounds on the numbers of atoms are thus determined by the trap anisotropy γ . For example, for $\gamma = 100$ (i.e., $a_\perp = 10a_z$) we have $N_j \ll 10^4 R_j^2$.

There is the critical number of atoms N_c such that the ^{85}Rb condensate, in the absence of the other isotope, is unstable with respect to collapse for $N_{85} > N_c$. By setting $g_{12} = 0$ in the two-dimensional system (6), we obtain the following expression for the critical number of the ^{85}Rb atoms necessary for collapse (in the absence of the other isotope):

$$N_c = \frac{2\pi I_0}{|g_{11}|} = \frac{\sqrt{\pi} I_0}{2\sqrt{2}} \frac{a_{1,z}}{|a_1|} = \kappa_{2D} \frac{a_{1,z}}{|a_1|}, \quad (9)$$

where $\kappa_{2D} = 1.167$. In derivation of formula (9) we have used the well-known condition for collapse in the critical nonlinear Schrödinger equation (for details consult Ref. [21]) and that the number of particles N_0 in the so-called Townes soliton is $N_0 = 2\pi I_0$, where $I_0 = 1.862$.

It is important to notice that both the upper bound (8) on the admissible numbers of atoms and the threshold number for collapse (9) in the ^{85}Rb condensate are proportional to the trap size in z -direction. Thus, taking a bigger pancake trap (with the same γ) will relax the bounds on the numbers of atoms. The threshold for collapse in the mixture of the two isotopes of Rubidium also depends on the number of atoms of the ^{87}Rb isotope. However, we have found numerically that this dependence is very weak (the correction does not exceed 5% for the numbers of atoms used below), therefore, the threshold given by (9) can be taken as a good approximation. For example, for the pancake trap with $a_z = 10\mu\text{m}$, used above, the threshold for collapse is $N_c = 535$.

Finally, let us comment on the validity of the approximate 2D system for description of the collapse instability in the mixture. First of all, one may point out that the threshold value for collapse of the mixture in the pancake trap determined from the full three-dimensional system (1) may turn out to be lower than that predicted by the two-dimensional approximation, as it is true, for instance, for the single species condensate of ^{85}Rb . Indeed, in the latter case, the exact (i.e., 3D) threshold can be written as $N_c = \kappa(\gamma)a_z/|a_1|$ [22]. Using the numerically found values of $\kappa(\gamma)$ from Ref. [22], we conclude that $\kappa(\gamma) < \kappa_{2D}$ for any $\gamma > 1$, i.e., this inequality holds for any pancake trap. As $\gamma \rightarrow \infty$, the function $\kappa(\gamma)$ slowly tends to κ_{2D} . For example, for the trap with $a_z = 10\mu\text{m}$ and $\gamma = 100$ we have $\kappa(100) = 1.1$ [22] what gives 95% (506 atoms) of the threshold given by formula (9).

Nevertheless, in the pancake trap, the instability which is solely due to the three-

dimensionality is weak if the conditions given by (8) are satisfied and the numbers of atoms are not much greater than the corresponding instability threshold. This conclusion follows from the general discussion of the 2D approximation, which is placed in appendix A. Here we note also that the instability rate due to the 3D effects decreases with increase of the trap anisotropy γ (since it enters the r.h.s.'s of the conditions (8)). Therefore, in a sufficiently anisotropic pancake trap, the 3D collapse instability below the threshold of the 2D collapse does not have enough time to develop on the time scale set by the two-dimensional system (6) and, hence, its effect on the solutions can be neglected. In fact, the time necessary for such a weak instability to develop may exceed the life-time of the condensates in the mixture.

It is, however, the *dynamics* of a collapsing condensate in the pancake trap that cannot be treated in the framework of the two-dimensional approximation and requires the full 3D analysis due to violation of one of the two conditions (8) in the collapsing condensate. Thus we will not discuss such dynamics (for details on the two-species collapse consult, for instance, Ref. [20]).

In the case of the two-species BEC of ^{85}Rb and ^{87}Rb , there is a stable state in the mixture, predicted by the 2D system (6) for the numbers of atoms slightly lower than the collapse instability (see the next section), which violates the applicability conditions (8) for modest pancake traps ($\gamma \leq 100$) due to sharp contraction of the ^{85}Rb condensate. The sharp decrease of the ^{85}Rb condensate size R_1 , predicted by the system (6), requires large trap anisotropy γ for the 2D system to sustain its validity. Therefore, for the current experimental traps, the very existence of such exotic states requires the full 3D analysis and thus is beyond the 2D approximation adopted in the present paper. We will not discuss such states either.

Therefore, for the current experimental pancake traps, the applicability of the approximate 2D system (6) is limited by the threshold of formation of the contracted states in ^{85}Rb condensate (which is slightly lower than the collapse instability threshold in 2D). In the next section we discuss the ground states in the mixture for the allowed numbers of atoms and their deformations due to instabilities predicted by the 2D model, such as the symmetry-breaking transition. Such instabilities are much stronger than those due to the three-dimensional effects and, consequently, are observed on much shorter time scale (consult also appendix A).

III. GROUND STATES IN THE MIXTURE OF TWO ISOTOPES OF RUBIDIUM

Now we turn to the numerical solution of the system (6) to find possible ground states in the BEC mixture of the two isotopes. The stationary solutions are sought for in the usual form:

$$\psi_1 = e^{-i\mu_1 T} U_1(\rho), \quad \psi_2 = e^{-i\mu_2 T} U_2(\rho), \quad (10)$$

where μ_1 and μ_2 are the dimensionless chemical potentials for the two species. We have used the gradient method for the constrained energy minimization to find $U_1(\rho)$ and $U_2(\rho)$ minimizing the energy functional

$$\mathcal{E} = \int d^2\boldsymbol{\rho} \left\{ |\nabla_{\perp}\psi_1|^2 + |\nabla_{\perp}\psi_2|^2 + \rho^2(\lambda_1^2|\psi_1|^2 + \lambda_2^2|\psi_2|^2) + \frac{g_{11}}{2}|\psi_1|^4 + \frac{g_{22}}{2}|\psi_2|^4 + g_{12}|\psi_1\psi_2|^2 \right\} \quad (11)$$

for fixed numbers of atoms $N_1 = \int d^2\boldsymbol{\rho} |\psi_1|^2$ and $N_2 = \int d^2\boldsymbol{\rho} |\psi_2|^2$.

A. Ground states for repulsive interspecies interaction

Let us start with considering the BEC mixture of ^{85}Rb and ^{87}Rb atoms with the repulsive interspecies interaction. First of all, we have found the axially symmetric ground states via the energy minimization restricted to the space of the axially symmetric functions. It is important to know if the symmetric states are stable. The stability analysis is based on the method of Refs. [23, 24], whose adaptation to our problem is described in appendix B. We have found that the axially symmetric ground state of the mixture suffers from the dipole-mode symmetry-breaking instability for sufficiently large number of atoms in the ^{87}Rb condensate and not too large numbers of atoms in the ^{85}Rb condensate ($N_{85} \leq 500$). The symmetry breaking instability was previously discussed for the case of BEC mixtures in Refs. [12, 13, 14, 15, 16]. The novelty here lies in the fact that one of the condensates has attractive atomic interaction. For instance, the separation criterion of Ref. [11] for a BEC mixture in the box, i.e., $g_{12} > \sqrt{g_{11}g_{22}}$, loses its meaning since in our case $g_{11}g_{22} < 0$ and, *a priori*, it is not evident that the isotopes would separate at all.

The axially symmetric ground states on the threshold of the symmetry-breaking instability for various numbers of atoms are shown in figure 1. It should be stressed that there are three types of the *stable* axially symmetric states in the system for smaller numbers

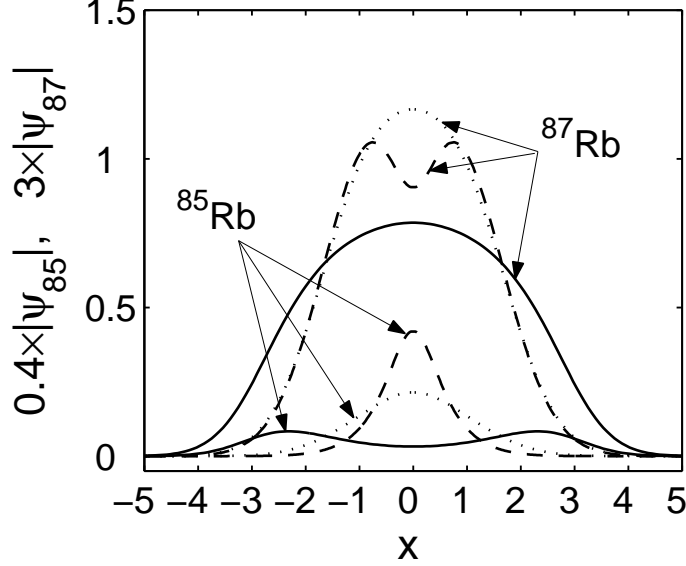


FIG. 1: The three types of the axially symmetric state in the mixture of ^{85}Rb and ^{87}Rb isotopes on the threshold of the symmetry-breaking instability. The one-particle wave functions are shown (scaled for better visibility as is indicated on the y -axis). The numbers of atoms are as follows. Solid lines: $N_{85} = 100$ and $N_{87} = 17412$; dotted lines: $N_{85} = 300$ and $N_{87} = 2042$; and dashed lines: $N_{85} = 450$ and $N_{87} = 894$.

of atoms, which correspond (and are similar) to the threshold states shown in figure 1: (i) when the isotopes are strongly mixed (the two condensates have bell-shaped form, the dotted lines), (ii) when the ^{85}Rb isotope is on the surface of ^{87}Rb ($|\psi_1|$ has a local minimum at the center, the solid lines), and (iii) when the ^{87}Rb isotope is on the surface of ^{85}Rb isotope ($|\psi_2|$ has a local minimum at the center, the dashed lines).

The threshold of the symmetry-breaking instability strongly depends on the numbers of atoms and corresponds to appearance of a zero dipole mode (which pertains to the orbital operator Λ_{11} , consult appendix B). From the energetic point of view, the separation takes place when the energy gain due to the intraspecies interaction in the strongly mixed state is higher than the kinetic energy (quantum pressure) at the interface between the separated condensates. The corresponding symmetry-breaking diagram, found numerically, is given in figure 2.

Though all three types of the axially symmetric ground states discussed above suffer from the symmetry-breaking instability with increase of the number of atoms of the ^{85}Rb isotope

(for sufficiently large number of atoms of the ^{87}Rb isotope) the symmetry-restored states (found to the right of the phase separation curve in figure 2), which result from further increase of the number of ^{85}Rb atoms, are of type (iii), i.e., when the ^{87}Rb isotope is on the surface of the ^{85}Rb isotope.

In the reduced 2D system (6), with further increase of the number of ^{85}Rb atoms the symmetry-restored state of type (iii) is followed by a sharp contraction of the ^{85}Rb condensate and subsequent collapse instability at $N_{85} \approx 535$ (the threshold slightly decreases with increase of the number of ^{87}Rb atoms). The collapse instability is due to appearance of the axially symmetric unstable mode (i.e., the linear mode with the orbital number $l = 0$, see appendix B).

Thus, right before the collapse instability the size of the ^{85}Rb condensate first decreases to a fraction of the trap size a_{\perp} . However, depending on the trap anisotropy γ , such a state may violate the first of the two applicability conditions (8) for the 2D approximation. For example, our estimates show that accurate description of this effect requires the full 3D analysis for the pancake traps with $\gamma \leq 100$. For observation of this effect, much more anisotropic pancake traps are required, which are not used in the current experiments. Thus we will not discuss the effect any further. There is also an implication on the validity of a part of figure 2 for the current pancake traps: the 2D approximation for the pancake trap with $\gamma \leq 100$ is not valid for description of the symmetric ground states to the right of the separation curve except a narrow strip immediately after it (with the width equal to a dozen of atoms on the N_{85} axis).

The symmetry-breaking ground states are illustrated in figures 3 and 4, where we show the contour lines of the order parameters (ranging from the maximum to a half of its value at a constant step) for ^{85}Rb (solid lines) and ^{87}Rb (dashed lines). We have found that it is the ^{85}Rb condensate that is expelled from the center of the trap in the symmetry-breaking states. It is seen that for comparable numbers of atoms of the two species it is the ^{87}Rb condensate that suffers the strongest deformation from the bell-shaped form, while for $N_{87} \gg N_{85}$ the ^{85}Rb condensate is strongly deformed. Here we note that the asymmetric ground state of the mixture is degenerated, as it possesses the rotational zero mode. In other words, the maximum of the order parameter of ^{85}Rb can have arbitrary position angle on the surface of the ^{87}Rb condensate.

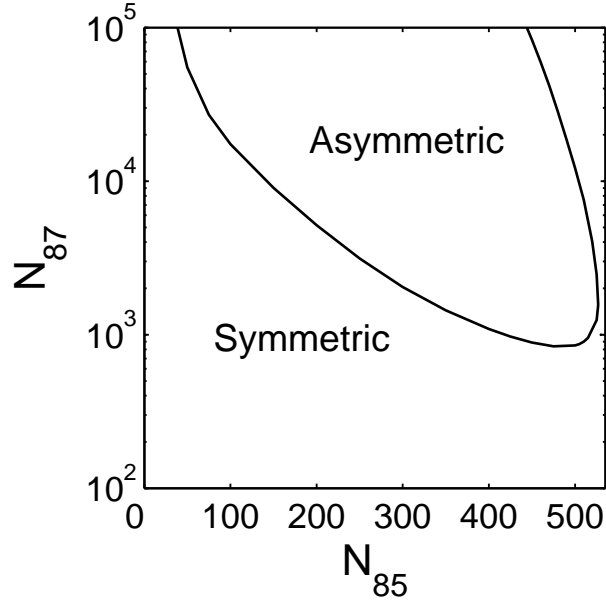


FIG. 2: The symmetric vs. asymmetric ground state diagram. The interaction coefficients are: $g_{11} = -0.0219$, $g_{22} = 0.0068$, and $g_{12} = 0.012$ (computed for the default values of the scattering lengths and $a_{1,z} = 10 \mu\text{m}$). The logarithmic (base 10) scale is used for the ^{87}Rb -axis.

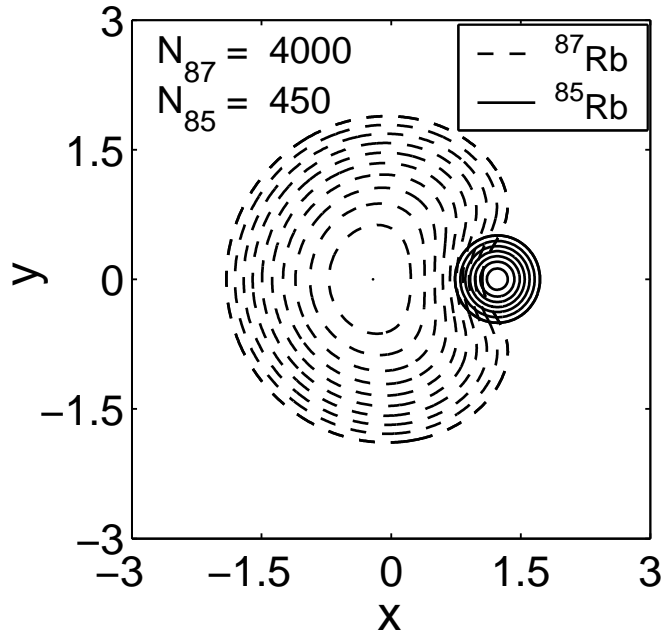


FIG. 3: The symmetry-breaking ground state for not too large number of ^{87}Rb atoms. For each of the two condensates, the equidistant level curves ranging from the maximum of the order parameter to a half of its value are shown.

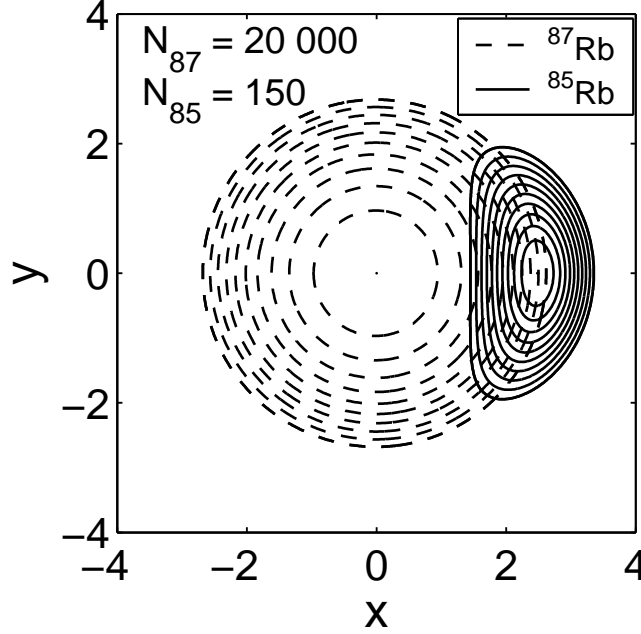


FIG. 4: The asymmetric ground state for very large number of ^{87}Rb atoms. The equidistant level curves are shown with the range defined as in the previous figure.

B. Ground states for attractive interspecies interaction

Now let us consider the BEC mixture of the two isotopes when the interspecies interaction is attractive, which can be experimentally realized by using the Feshbach resonance [8]. It is convenient to measure the interspecies interaction coefficient g_{12} in terms of the interaction coefficient g_{11} of the ^{85}Rb isotope. We have found that the condensates do not separate in this case and assume the axially symmetric ground state up to the collapse instability threshold. Such ground states are illustrated in figure 5, where we plot the appropriately scaled one-particle wave-functions for the two condensates. Note the local peak at the center of the ^{87}Rb condensate. Appearance of this peak is easy to understand, for instance, when the Thomas-Fermi limit applies to the ^{87}Rb condensate (which corresponds to the picture in the lower panel of figure 5). Indeed, if $N_{87} \gg N_{85}$, then in the zero-order approximation one can neglect the contribution from the interspecies interaction term $g_{12}|\psi_1|^2$ in equation (6b) for the ^{87}Rb condensate in the region away from the trap center. Thus, in the zero-order approximation, the ^{87}Rb condensate has the Thomas-Fermi ground state independently of the state of the other isotope. Therefore the effect of the cross-interaction term $g_{12}|\psi_2|^2$ in

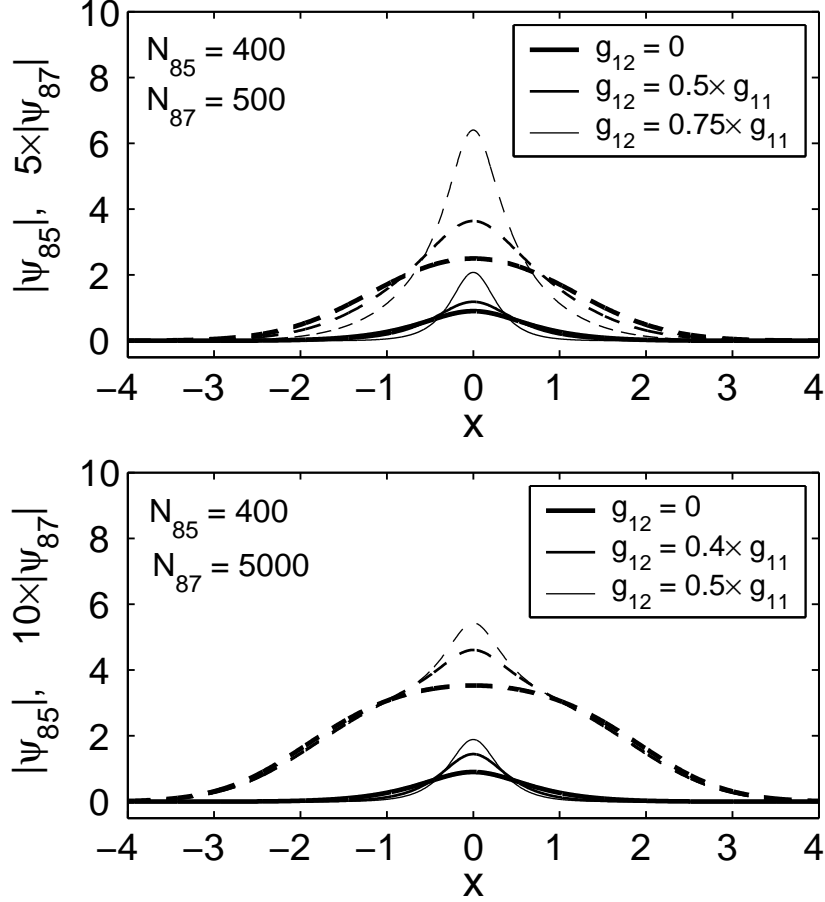


FIG. 5: Stable ground states of the BEC mixture for the attractive interspecies interactions. The one-particle wave functions (scaled for better visibility as indicated along the y -axis) are shown. In both panels, the solid lines correspond to the ^{85}Rb isotope and the dashed lines to the ^{87}Rb isotope.

the equation for the ^{85}Rb condensate (6a) is now similar to that of an additional potential. In the next order of approximation, the order parameter ψ_2 of the ^{87}Rb condensate is a sum of the two terms: one is the original Thomas-Fermi function and the other one represents its deformation at the center of the trap. The latter is determined by the order parameter of the ^{85}Rb condensate.

It should be noted that, notwithstanding the attraction in the ^{85}Rb condensate and the attractive interspecies interaction, the ground states shown in figure 5 are not self-bound (i.e., they are not solitons): relaxation of the trap results in spreading of the condensates.

Finally, lowering of the interspecies interaction coefficient g_{12} to the sufficiently large

negative values results in sharp contraction of the ^{85}Rb condensate which is followed by the collapse instability. This contraction of the *stable* ground state of the ^{85}Rb condensate to a fraction of the trap size is due to the presence of the other condensate, since the size of a stable single species BEC in 2D is always on the order of the trap size.

Thus, as in the case of the repulsive interspecies interactions, the collapse instability in the mixture is preceded by a sharp decrease of the ^{85}Rb condensate size. Therefore, depending on the trap anisotropy γ , its description may take us beyond the 2D approximation adopted in this paper. For most of the current pancake traps $\gamma \leq 100$, consequently the description of the ground state in the mixture which is on the border of the collapse instability requires the full three-dimensional analysis.

We note, however, that for small values of $|g_{12}|$ the stable symmetric ground states predicted by the 2D approximation and illustrated in figure 5 can be experimentally observed in the current pancake traps with $\gamma \sim 100$. In such experiment, the number of ^{85}Rb atoms should be below the threshold value $N_c = N_c(N_{87})$ which, for fixed g_{12} , decreases only by a few percent from the value given by formula (9) with increase of the number of ^{87}Rb atoms.

IV. CONCLUSION

We have studied the ground state in the BEC mixture of two isotopes of Rubidium in the pancake trap for repulsive and attractive interspecies interactions and fixed (default) intraspecies interactions.

In the case of repulsion between the two species, there is the symmetry-breaking deformation of the ground state due to the dipole-mode instability, whose threshold strongly depends on the numbers of atoms of the two isotopes. For small numbers of atoms, i.e., below the symmetry-breaking instability threshold, the stable axially symmetric ground state has the form of either the strongly mixed state of the species (with the order parameters of the two condensates having the bell-shaped form) or the state where one of the condensates forms a circular strip on the surface of the other.

For attractive interspecies interaction, the condensates assume the axially symmetric ground states for all numbers of atoms where the 2D approximation is valid. For small values of the (negative) interspecies interaction coefficient $|g_{12}|$ the mixture is stable for the numbers of ^{85}Rb atoms below the critical value $N_c = N_c(N_{87})$ which is a few percent

lower than the collapse instability threshold for a single species condensate of ^{85}Rb (i.e., for $g_{12} = 0$).

Finally, for the pancake traps with the anisotropy $\gamma \leq 100$, the 2D approximation for the attractive as well as repulsive mixture is violated at the numbers of atoms in the ^{85}Rb condensate just below the collapse instability in the 2D model due to the sharp contraction of the ^{85}Rb condensate. This is quite dissimilar to the case of the single species BEC of ^{85}Rb , where the collapse sets in at a state which has the size comparable to the trap size in the pancake plane. Thus, the investigation of the actual ground state of the mixture in such pancake traps at the numbers of atoms close to the collapse instability requires the full three-dimensional analysis and is beyond the approach adopted in the present paper. This sets a direction for the future research.

Acknowledgements

This work was supported by the FAPESP of Brazil. A.M.K. would like to thank the Instituto de Física Teórica - UNESP for kind hospitality. We are grateful to the referee for the suggestions which resulted in significant improvement of the presentation.

APPENDIX A: DERIVATION OF THE TWO-DIMENSIONAL APPROXIMATION

The system (1) can be rewritten in the following form:

$$i\hbar\partial_t\Psi_1 = (H_{1z} + H_{1\perp} + G_{11}|\Psi_1|^2 + G_{12}|\Psi_2|^2)\Psi_1, \quad (\text{A1})$$

$$i\hbar\partial_t\Psi_2 = (H_{2z} + H_{2\perp} + G_{22}|\Psi_2|^2 + G_{12}|\Psi_1|^2)\Psi_2, \quad (\text{A2})$$

where we have introduced the linear operators corresponding to the quantum motion along z -axis and on the (x, y) -plane in the trap:

$$H_{jz} = -\frac{\hbar^2}{2m_j}\frac{\partial^2}{\partial z^2} + V_{jz}(z), \quad H_{j\perp} = -\frac{\hbar^2}{2m_j}\nabla_{\perp}^2 + V_{j\perp}(\mathbf{r}_{\perp}), \quad j = 1, 2.$$

The solution to equations (A1)-(A2) can be expanded over the eigenfunctions of the linear operators H_{1z} and H_{2z} as follows: $\Psi_j = \Psi_{j0}(z, \mathbf{r}_{\perp}, t) + \hat{\Psi}_j(z, \mathbf{r}_{\perp}, t)$, $j = 1, 2$, where $\Psi_{j0} \equiv e^{-iE_{j0}t/\hbar}f_j(z)\Phi_j(\mathbf{r}_{\perp}, t)$, with $f_j(z)$ being the normalized eigenfunction of the ground

state, $H_{jz}f_j(z) = E_{j0}f_j(z)$, while the second term, $\hat{\Psi}_j$, is the projection of order parameter Ψ_j on the subspace orthogonal to the ground state.

We can expand the system (A1)-(A2) in similar way using the projectors Π_1 and Π_2 on the ground states of H_{1z} and H_{2z} , respectively. Application of these projectors to equations (A1)-(A2) leads to the system describing evolution of the projection of the order parameters for the two species on the respective ground states:

$$i\hbar\partial_t\Phi_1 = \left(H_{1\perp} + \tilde{G}_{11}|\Phi_1|^2 + \tilde{G}_{12}|\Phi_2|^2 + \Delta_1\right)\Phi_1 + \mathcal{F}_1, \quad (\text{A3})$$

$$i\hbar\partial_t\Phi_2 = \left(H_{2\perp} + \tilde{G}_{22}|\Phi_2|^2 + \tilde{G}_{12}|\Phi_1|^2 + \Delta_2\right)\Phi_2 + \mathcal{F}_2, \quad (\text{A4})$$

where $\tilde{G}_{ij} = G_{ij}\langle f_i^2 f_j^2 \rangle$, with $\langle F \rangle \equiv \int F dz$,

$$\Delta_j = G_{jj}\langle f_j^2(2f_i\text{Re}\{\Phi_j\hat{\Psi}_j^*\} + |\hat{\Psi}_j|^2) \rangle + G_{j,3-j}\langle f_j^2(2f_{3-j}\text{Re}\{\Phi_{3-j}\hat{\Psi}_{3-j}^*\} + |\hat{\Psi}_{3-j}|^2) \rangle, \quad (\text{A5})$$

and

$$\mathcal{F}_j = G_{jj}\langle f_j|\Psi_j|^2\hat{\Psi}_j \rangle + G_{j,3-j}\langle f_j|\Psi_{3-j}|^2\hat{\Psi}_j \rangle. \quad (\text{A6})$$

On the other hand, the equations describing evolution of the projections of the order parameters on the orthogonal subspaces are derived by application of the complementary projectors Q_j , $Q_j \equiv \mathbb{1} - \Pi_j$, to the system (A1)-(A2):

$$i\hbar\partial_t\hat{\Psi}_1 = \left(\tilde{H}_{1z} + H_{1\perp}\right)\hat{\Psi}_1 + Q_1\{G_{11}|\Psi_1|^2\Psi_1 + G_{12}|\Psi_2|^2\Psi_1\}, \quad (\text{A7})$$

$$i\hbar\partial_t\hat{\Psi}_2 = \left(\tilde{H}_{2z} + H_{2\perp}\right)\hat{\Psi}_2 + Q_2\{G_{22}|\Psi_2|^2\Psi_2 + G_{12}|\Psi_1|^2\Psi_2\}, \quad (\text{A8})$$

where $\tilde{H}_{jz} = H_{jz} - E_{j0}$.

Let us estimate the orders of magnitude of the nonlinear terms in equations (A3)-(A4) and (A7)-(A8) under the condition that the nonlinear terms in the system (A1)-(A2) are much smaller than the characteristic difference $\Delta E \sim \hbar\omega_z$ between the eigenvalues of each of the two linear operators H_{1z} and H_{2z} (i.e., the conditions (3) are satisfied). Below we will not distinguish between the quantities with different indexes, since all quantities of the same kind are of the same order of magnitude. Introduce a small parameter ϵ as the ratio of the nonlinear terms in the system (A3)-(A4) to ΔE , that is

$$\epsilon = \frac{\tilde{G}|\Phi|^2}{\Delta E} = \frac{G\langle f^4 \rangle |\Phi|^2}{\Delta E}. \quad (\text{A9})$$

Note that $\langle f^4 \rangle \sim f^2$ since the integral of f^2 over z is of order 1. It is the smallness of ϵ , supposed in (3), that justifies the transition to the two-dimensional approximation.

Indeed, the order of the correction $\hat{\Psi}$ to the factorized wave function can be found by equating the orders of the inhomogeneous term and the linear term $H_z + H_\perp$ in (A7)-(A8), where, as in (A3)-(A4), we have again $H_\perp \hat{\Psi} \sim \epsilon \Delta E \hat{\Psi}$ and H_\perp can be neglected compared with $H_z \sim \Delta E$. Therefore, we get $\Delta E \hat{\Psi} \sim GQ\{|f\Phi|^2 f\Phi\} \sim \epsilon \Delta E f\Phi$ and, hence, $\hat{\Psi} \sim \epsilon f\Phi$. From this we obtain the estimates for the terms given by equations (A5) and (A6): $\Delta \sim G\langle f^2 f\Phi \hat{\Psi} \rangle \sim \epsilon G f^2 \Phi^2 \sim \epsilon^2 \Delta E$ and $\mathcal{F} \sim G\langle f(f\Phi)^2 \epsilon f\Phi \rangle \sim \epsilon G f^2 \Phi^2 \Phi \sim \epsilon^2 \Phi \Delta E$.

Throwing away the terms of the order ϵ^2 from equations (A3)-(A4) and changing to the dimensionless variables given by (5) we arrive at the system (6). The projection of the order parameter Ψ_j on the orthogonal subspace, $\hat{\Psi}_j$, is of order ϵ and can be neglected compared to the factorized wave function $f_j \Phi_j$. We conclude that, under the conditions (3), nonlinearity plays significant role only on the pancake plane (x, y) .

Two comments are in order on the two-dimensional approximation described above. First, the effects due to three-dimensionality of the mixture will be of order ϵ^2 , the same order as the terms we have thrown out from the system (A3)-(A4), thus they will give a significant contribution to the dynamics only on the time scale of order ϵ^{-2} , much longer than the time scale of the nonlinear effects in 2D, which is of order ϵ^{-1} . Second, a similar 2D approximation will be valid for the linearized system which describes the evolution of a small perturbation of the solution. Thus, any instability in the mixture which is solely due to its three-dimensionality will be of order ϵ^2 and will not play any role on the time scale we consider.

The latter comment concerns, for instance, the instability due to collapse in 3D: although the 3D threshold value of the number of atoms in the mixture necessary for collapse may turn out to be lower than that in the 2D approximation, as it is true for the single species condensate of ^{85}Rb , the corresponding instability rate (proportional to the unstable eigenvalue) will be of order ϵ^2 and will not be noticed on the time scale we consider.

APPENDIX B: THE LINEAR STABILITY ANALYSIS

The linear stability analysis is based on the consideration of evolution of a linear perturbation $u_1 = u_1(\boldsymbol{\rho}, T)$ and $u_2 = u_2(\boldsymbol{\rho}, T)$ of the stationary state $(U_1(\rho), U_2(\rho))$. The evolution equations for the perturbation are derived by linearization of the original system (system (6)) about the stationary solution. One looks for the eigenfrequencies ω of the resulting

linear system by setting $u_j = e^{-i\omega t}(X_j(\boldsymbol{\rho}) + iY_j(\boldsymbol{\rho}))$, $j = 1, 2$. Appearance of an imaginary eigenfrequency means instability. In particular, by writing the perturbed solution as

$$\psi_j = e^{-i\mu_j T}(U_j(\rho) + u_j(\boldsymbol{\rho}, T)), \quad j = 1, 2, \quad (\text{B1})$$

using this in the system (6) and keeping only the linear terms in u_1 and u_2 we arrive at the following eigenvalue problem (consult also Refs. [23, 24]):

$$\Lambda_0 \begin{pmatrix} Y_1 \\ Y_2 \end{pmatrix} = -i\omega \begin{pmatrix} X_1 \\ X_2 \end{pmatrix}, \quad \Lambda_1 \begin{pmatrix} X_1 \\ X_2 \end{pmatrix} = i\omega \begin{pmatrix} Y_1 \\ Y_2 \end{pmatrix}, \quad \Lambda_n = \begin{pmatrix} L_{n1} & 0 \\ 0 & L_{n2} \end{pmatrix}. \quad (\text{B2})$$

Here ($j = 1, 2$):

$$L_{0j} = -\mu_j - \nabla_{\perp}^2 + \sum_{m=1,2} g_{jm} U_m^2(\rho) + \lambda_j^2 \rho^2, \quad (\text{B3})$$

$$L_{1j} = -\mu_j - \nabla_{\perp}^2 + \sum_{m=1,2} g_{jm} U_m^2(\rho) + 2g_{jj} U_j^2(\rho) + \lambda_j^2 \rho^2.$$

Expansion of the eigenvalue problem (B2) in the Fourier series with respect to the polar angle θ leads to an infinite series of one-dimensional eigenvalue problems of similar form for the orbital projections of the vectors $(X_1, X_2)^T$ and $(Y_1, Y_2)^T$,

$$X_j = \sum_{l \geq 0} X_{jl}(\rho) e^{il\theta} + \text{c.c.}, \quad Y_j = \sum_{l \geq 0} Y_{jl}(\rho) e^{il\theta} + \text{c.c.}, \quad j = 1, 2, \quad (\text{B4})$$

with the orbital operators defined by $\Lambda_{0l} = \Lambda_0(\nabla_{\perp}^2 \rightarrow \nabla_{\rho}^2 - l^2/\rho^2)$ and $\Lambda_{1l} = \Lambda_1(\nabla_{\perp}^2 \rightarrow \nabla_{\rho}^2 - l^2/\rho^2)$, where $\nabla_{\rho}^2 \equiv \partial_{\rho}^2 + \rho^{-1}\partial_{\rho}$. However, only a few of these 1D eigenvalue problems need to be considered to decide on stability of the axial ground state. Indeed, first, as follows from the general criterion for stability of the ground state in a system of nonlinear Schrödinger equations [24], in the two-component system the axial ground state is unstable if there are at least three negative eigenvalues of the operator Λ_1 . For instance, if each of the first three orbital operators Λ_{1l} , $l = 0, 1, 2$ has a negative eigenvalue, then the ground state is unstable. Second, as the orbital operators satisfy the obvious inequality $\Lambda_{1l_2} \geq \Lambda_{1l_1}$ (understood as the inequality for the mean values) for $l_2 \geq l_1$, it is sufficient to consider just three orbital problems arising from (B2) with the orbital numbers $l = 0, 1, 2$. This is the approach we adopted.

Finally, we would like to mention that the linear stability is closely related to the energy minimization (consult also Refs. [23, 24]). Indeed, the operator Λ_0 is non-negative (it has

two zero modes due to the phase invariance of the system (6)). Thus, from the energetic point of view, a negative eigenvalue of the operator Λ_1 corresponds to a negative direction in the free energy functional, defined here as the Lagrange-modified energy functional: $\mathcal{F} \equiv \mathcal{E} - \mu_1 N_1 - \mu_2 N_2$, evaluated at the axially symmetric state $(U_1(\rho), U_2(\rho))$, since the operator Λ_1 enters the second-order term in the free energy expansion with respect to the perturbation $\hat{u}_j = X_j(\boldsymbol{\rho}) + iY_j(\boldsymbol{\rho})$, $j = 1, 2$:

$$\delta^2 \mathcal{F} = 2 \int d^2 \boldsymbol{\rho} \left\{ (Y_1, Y_2) \Lambda_0 \begin{pmatrix} Y_1 \\ Y_2 \end{pmatrix} + (X_1, X_2) \Lambda_1 \begin{pmatrix} X_1 \\ X_2 \end{pmatrix} \right\}. \quad (\text{B5})$$

Taking into account that there are two independent constraints on the numbers of atoms in the two species we conclude that only two negative directions may be eliminated by the energy dependence on the numbers of atoms. Therefore, for fixed numbers of atoms, the axially symmetric state is definitely not an energy minimum if there are three (or more) negative eigenvalues of the operator Λ_1 . This explains the physical origin of the above mentioned sufficient condition for instability. We note also that the dipole-mode instability (i.e., existence of the unstable orbital mode with the orbital number $l = 1$) simply means appearance of an asymmetric state which minimizes the energy, i.e., the symmetry-breaking transition.

-
- [1] C. J. Myatt, E. A. Burt, R. W. Ghrist, E. A. Cornell, and C. E. Wieman, Phys. Rev. Lett. **78**, 586 (1997).
 - [2] D. S. Hall, M. R. Matthews, J. R. Ensher, C. E. Wieman, and E. A. Cornell, Phys. Rev. Lett. **81**, 1539 (1998).
 - [3] J. Stenger, S. Inouye, D. M. Stamper-Kurn, H.-J. Miesner, A. Chikkatur, and W. Ketterly, Nature **396**, 345 (1998).
 - [4] H.-J. Miesner, D. M. Stamper-Kurn, J. Stenger, S. Inouye, A. P. Chikkatur, and W. Ketterle, Phys. Rev. Lett. **82**, 2228 (1999).
 - [5] P. Maddaloni, M. Modugno, C. Fort, F. Minardi, and M. Inguscio, Phys. Rev. Lett. **85**, 2413 (2000).
 - [6] G. Modugno, M. Modugno, F. Riboli, G. Roati, and M. Inguscio, Phys. Rev. Lett. **89**, 190404 (2002).

- [7] Z. Hadzibabic, C. A. Stan, K. Dieckmann, S. Gupta, M.W. Zwierlein, A. Görlitz, and W. Ketterle, Phys. Rev. Lett. **88**, 160401 (2002).
- [8] J. P. Burke, Jr., J. L. Bohn, B. D. Esry, and Chris H. Greene, Phys. Rev. Lett. **80**, 2097 (1998).
- [9] I. Bloch, M. Greiner, O. Mandel, Th. W. Hänsch, and T. Esslinger, Phys. Rev. A **64**, 021402 (2001).
- [10] S. L. Cornish, N. R. Claussen, J. L. Roberts, E. A. Cornell, and C. E. Wieman, Phys. Rev. Lett. **85**, 1795 (2000).
- [11] P. Ao and S. T. Chui, Phys. Rev. A **58**, 4836 (1998).
- [12] P. Öhberg and S. Stenholm, Phys. Rev. A **57**, 1272 (1998).
- [13] D. Gordon and C. M. Savage, Phys. Rev. A **58**, 1440 (1998).
- [14] B. D. Esry and C. H. Greene, Phys. Rev. A **59**, 1457 (1999).
- [15] J. G. Kim and E. K. Lee, Phys. Rev. E **65**, 066201 (2002).
- [16] A. A. Svidzinsky and S. T. Chui, Phys. Rev. A **67**, 053608 (2003).
- [17] H. Pu and N. P. Bigelow, Phys. Rev. Lett. **80**, 1134 (1998)
- [18] Th. Busch, J. I. Cirac, V. M. Pérez-García, and P. Zoller, Phys. Rev. A **56**, 2978 (1997).
- [19] L. P. Pitaevskii and S. Stringari, *Bose-Einstein condensates in gases* (Cambridge University Press, Cambridge 2003).
- [20] S. K. Adhikari, Phys. Rev. A **63**, 043611 (2001); J. Phys. B: At. Mol. Opt. Phys. **34**, 4231 (2001).
- [21] G. Fibich and G. Papanicolaou, SIAM J. Appl. Math. **60**, 183 (1999).
- [22] A. Gammal, T. Frederico, and L. Tomio, Phys. Rev. A **64**, 055602 (2001); A. Gammal, L. Tomio, and T. Frederico, Phys. Rev. A **66**, 043619 (2002).
- [23] E. A. Kuznetsov, A. M. Rubenchik, and V. E. Zakharov, Phys. Rep. **142**, 103 (1986).
- [24] D. E. Pelinovsky and Yu. S. Kivshar, Phys. Rev. A **62**, 8668 (2000).